Pressure wave propagation induced by short circuits inside power transformers: Development of a simulation tool, comparisons with experiments and applications

Sébastien Muller, Margareta Petrovan-Boiarciuc and Guillaume Périgaud
SERGI Holding, 186 av. du Général de Gaulle,
P.O. Box 90, 78260 Achères, France
research@sergi-holding.com

Transformer explosion and its prevention is a complex industrial issue where various physical phenomena occur. To understand them, an experimental test campaign was performed by CEPEL on large scale transformers. It consisted in creating arcing in oil filled transformer tanks. The tests confirmed that the arc generates dynamic pressure waves that propagate in the oil. Reflections of these waves on the walls build up high static pressure to which transformer tanks can not withstand. This static pressure increase can be prevented by a quick oil evacuation triggered by the first dynamic pressure peak generated by the electrical arc. Moreover, a numerical tool was developed to simulate the phenomena highlighted during the tests and mainly the pressure wave propagation. It is thus based on a compressible two-phase flow modelling where viscous flow, electromagnetic, thermal and gravity effects are taken into account. The equations are solved using a finite volume method allowing computing complex 3D transformer geometries. Comparisons between the data obtained during the experiments and the results given by the simulations validated the model. It can be used to study transformer explosions as well as depressurisation induced by the explosion prevention technology based on a quick oil evacuation.

1. INTRODUCTION

A. GENERAL OVERVIEW

Privatisation of electricity companies leads to an electricity market that becomes more and more competitive. To limit costs, companies often reduce the investments by using aging equipments and by overloading the power transformers. Oil-filled transformer explosions are then more and more frequent and they result in dangerous fires, very expensive damages and possible environmental pollution. For all these reasons, transformer explosions and their prevention are becoming a critical industrial issue.

B. POWER TRANSFORMERS AND RELATED ITEMS

A power transformer is a device that transfers electrical energy from one circuit to another by magnetic coupling. Most of the time, it is composed of windings, placed in a tank filled with oil that ensures the cooling and electrical isolation of these windings (see Figure 1). Transformers can go up to 10 meters long and deal with power up to 1000 MVA. Explosions were found to occur when the transformer oil loses its dielectric properties (because of age,

Figure 1 Cut away view of three-phase oil-cooled transformer.

design errors, oil pollution, overloading, lack of maintenance...) leading to the occurrence of an electrical arc inside the transformer tank.

C. BACKGROUND IN TRANSFORMER EXPLOSIONS AND PREVENTIVE STUDIES

Several studies, experimental or computational, have been performed to understand the explosion process in order to establish strategies to prevent it.

An interesting test campaign was performed during the SEBK project. A first phase of the work [1] analyzed transformer oil vaporization, cracking and oil vapor explosion. Tests such as igniting a spark which could deliver up to 2 kJ in a small chamber (1-2 liters) showed the generation of highly flammable gas such as hydrogen and acetylene. Complementary tests showed that the amount of gas released is a very important parameter for the explosion load, an implication of this is that one very important risk reduction measure will be to minimise the amount of energy released in the electrical arc. The last phase of the project [2] was to simulate large scale transformer explosions. On that purpose, hydrogen gas was released in a transformer room (50 m^3) and oil transformer was sprayed in the room to represent gases from cracking of oil. This mixture was supposed to represent the gases generated by the cracking of oil and is ignited in the transformer room leading to a strong explosion, flames and overpressures up to 1.5 bar. Moreover, several systems based on spraying different mixtures (powder, water...) were tested in order to mitigate the effect of the explosion. Beside this experimental study, where the different phenomena that lead to the explosion were studied separately, a complete experimental study was performed by the CEPEL and the SERGI Holding Company. It consisted of arcing tests in industrial size oil-immersed transformers. Detailed results can be found in [2]. These tests highlight the physical phenomena modeled by the simulation tool presented in this paper and therefore the most important points are recalled in this paper.

Since live tests performed on real scale transformers are expensive and might be dangerous, an alternative is to study transformer explosions using computational simulations. The first models [4] considered the pressure uniform in the tank (0D model) and the tank oil incompressible. The authors compute the amplitude of the pressure peak induced by an arc in a gas blanket located in the top of the tank considering a semi

empirical energy conservation equation. The study detailed in [5] is based on similar hypotheses and considers that the tank expansion has to absorb the volume of the gas generated by the arc. Both works concluded that the best way to avoid an explosion is to give place to oil in order to absorb the oil expansion due to the electrical arc. A more elaborated method, detailed in [6] considers a 2D geometry and a potential flow model, using a source singularity to represent the arc. This incompressible and non-viscous model allows computing the deformation of the transformer tank considered as a thin-walled infinite cylinder shell. This model, completed with some empirical laws is also used in [7] to compute the overpressures generated by different arc characteristics for different tank geometry parameters.

Computation capabilities and CFD modeling progress over the last years now allow simulating industrial type problems with efficient unsteady 3D CFD models in reasonable time.

D. PAPER CONTENTS

The aim of this paper is to present the development of such a numerical tool able to describe unsteady non uniform pressure phenomena following the arc ignition and the influence on the pressure distribution of a mechanical device that evacuates the oil in order to prevent the explosion. This simulation tool will thus have to deal with 2 phase flows, unsteady compressible and viscous flow, electromagnetic forces, thermal and gravity effects and a 3D modeling.

This paper starts with a small review of the test campaign that was performed with the CEPEL on arcing inside large scale transformers. The main physical phenomena occurring during an explosion will be experimentally highlighted. In the second section, the physical modeling is addressed in details. The numerical method used to solve the physical partial differential equations is then presented. It is based on a finite volume strategy. The simulated pressure evolutions inside the tank are then compared to the data collected during the experiments. This will validate the simulation tool. Finally, simulations are performed on an industrial 200 MVA transformer geometry to evaluate a strategy based on a quick oil evacuation to prevent transformer explosions.

2. NOMENCLATURE

$\alpha_1\rho_1$	Gas partial mass	ρ	Mixture density
$\rho\vec{u}$	Mixture momentum	$\vec{u}$	Mixture velocity
E	Mixture total energy	ε	Mixture internal energy
P	Mixture pressure	α_1	Gas volume fraction
$\Phi_g^{u,E}$	Gravity terms	$\Phi_\mu^{u,E}$	Viscosity terms
Φ_T^E	Mixture Fourier's law	x, y, z	Spatial coordinates
u, v, w	Velocity components	$div\ (\cdot)$	Spatial divergence
$\partial\cdot/\partial\cdot$	Partial derivative	∇	Spatial gradient
$\otimes$	Tensor product	λ_i	Eigenvalue ith wave
Δt	Time step	$V(i)$	Neighbours to cell i
Ω_i	Volume of cell i	l	Cell edge length
$\vec{n}$	Normal to cell edge	ϕ_{ij}	Variable at cell edge
ϕ_i	Variable at cell i	ϕ^{n+1}	Variable at time n+1
ϕ^n	Variable at time n	$\overline{\overline{\mathrm{D}}}$	Deformation rate Tensor
$\overline{\overline{\tau}}$	Viscous Stress Tensor		

3. EXPERIMENTAL CAMPAIGN

A. CONTEXT

To understand the physical phenomena leading to a transformer explosion, a complete experimental test campaign was performed in collaboration with CEPEL, the Brazilian independent High Voltage Laboratory. Following a first test campaign performed in 2002 in collaboration with EDF on relatively small pole type transformers [8], the tests consisted in igniting an electrical arc inside real large transformers (up to 5.3 meters long).

Furthermore, since transformers explosions are very dangerous and uncontrollable, a transformer protection had to be installed during the experimental tests. This one, shown in green in Figure 2, is based on the direct mechanical response of a Depressurization Set (DS) to the tank inner pressure induced by electrical faults. The key of success is for the protection to depressurize the tank fast enough that is to say before it explodes. The following describes the tests performed in order to check it.

The aims of the experimental campaign were then to:

- Understand the physical phenomena occurring after an arc ignition inside a transformer,
- Test the efficiency of a transformer protection and understand its operation,
- Obtain experimental data in order to compare them with results obtained with simulations.

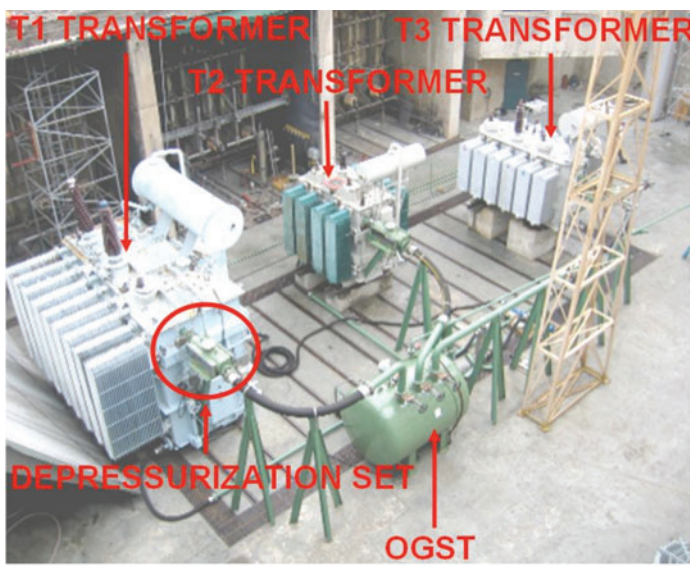

Figure 2 Test Configuration.

B. EXPERIMENTAL SETTINGS

34 live tests were performed on three standard transformers (T1, T2 and T3, see figure 2) with their internal equipments (windings, cables...) and equipped with various sensors. Their large sizes enabled the detailed study of the pressure non uniform distribution inside the tank. In these configurations the maximum distance between an electrical arc and the transformer protection (TP) ranged up to *8.5 meters (28 ft)*. These tests were also carried out to investigate the ability of a fast drain to depressurize a tank submitted to a low impedance

fault by measuring physical parameters such as pressure, gas temperature, applied current, arc voltage and tank acceleration.

1. Experimental Set

Each transformer was equipped with a Depressurization Set (DS). An Oil and Gas Separation Tank (OGST) was used to collect the oil and flammable gases expelled out of the transformer after the TP operation (see figure 3).

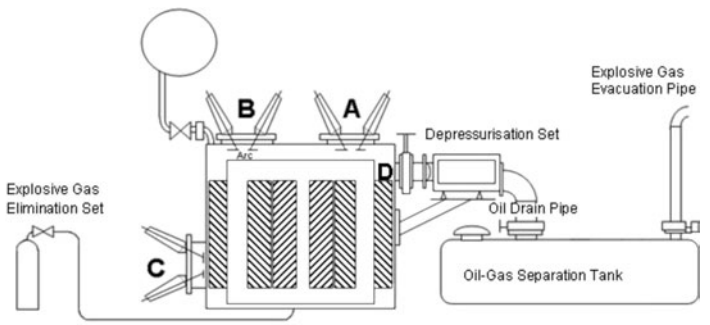

Figure 3 Live tests transformer principle drawings.

2. Experiments

To study in detail the pressure distribution and it evolution inside the tank, and to check that the protection reliability does not depend on the arc location inside the transformer tank, the electrical arcs were ignited, for each transformers, at three different locations, as shown in figure 3: on the top cover close to the Depressurization Set location (**position A**), on the top cover opposite the DS location (**position B**), and in the lower part of the tank opposite the DS location (**position C**). Position C was the harshest position to test because far from the DS and near the windings. Note that the **position D** is shown in figure 3, and is the location where the DS was installed.

Most of the tests were carried out with electrical arcs with currents ranging from *5* to *15 kA*, and fed for a duration of 83 milliseconds. This duration corresponds to the average response time of an old circuit breaker and was chosen to maximize the generated gas volume.

C. GENERATED GAS

During the CEPEL test campaign, the electrical arc produced from *1* to *2.3* m^3 (35 to 88 ft^3) of gas. This volume, measured at atmospheric pressure and temperature is plotted as a function of the arc energy in figure 4. The global trend (dotted curve) is drawn by the following equation:

$$V = 0.44 \ln(E + 5474.3) - 3.8$$

where E is the arc energy (in J) and V the generated volume (in m^3).

The gas volume generated during an electrical arc is thus a logarithmic function of the arc energy, which seems in accordance with the vaporization process and especially with the saturation of the vaporization for high energy arcs.

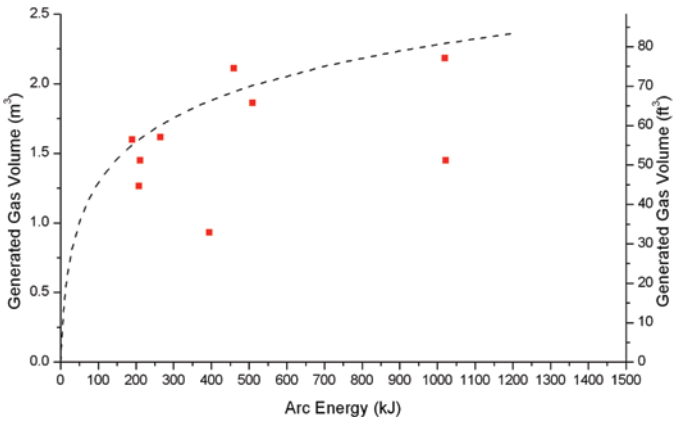

Figure 4 Generated gas volume vs. arc energy.

Indeed, after the arc has vaporized almost instantaneously an important gas volume, it stays in that volume using its energy to crack the oil vapor rather than continuing directly vaporizing the oil: this results in a smoother vaporization process. It explains the vaporization saturation process.

The first stage of vaporization process is almost instantaneous and because of the oil inertia, the gas is very quickly pressurized, generating one important pressure peak.

D. WAVE PROPAGATION AND STRUCTURE INTERACTION

At the beginning of the process, when the arc occurs, the tank is sealed and the vaporization generates a high pressure increase in the gas bubble. Let us see how the pressure increase evolves.

1. Pressure profile evolution at a single position

Figure 5 shows the pressure evolution at a sensor located close to the arc (position A) in the T3 transformer for an arc of *14 kA* located in A during *83 ms*.

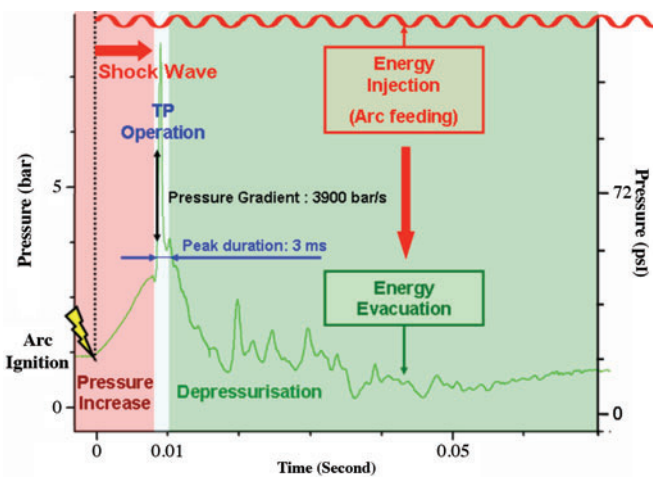

Figure 5 Pressure evolution close to the arc location after the arc ignition.

The different phases are detailed: after the arc ignition, the pressure locally rises and reaches a maximum level around 7 bars and then decreases back to the activation level after some milliseconds going through some secondary peaks lower than the first pressure maximum. Indeed, the shock wave, generated by the arc, propagates at a finite speed through the transformer tank, reaches the sensor with a pressure gradient of 3900 *bar/s* (56000 *psi/s*), reflects on the walls (which generates the secondary peaks) and triggers the fast drain which generates the global depressurization of the tank.

It can be noted that even if the arc is still fed for a long period, no other high pressure increases are noticed, this is mainly due to:

- the global depressurization induced by the drain,
- the saturation of the vaporization process: the under pressure gas bubble is created almost instantaneously and the energy of the arc is then used to crack the oil vapor without increasing the pressure.

2. Pressure wave propagation

In figure 6, experimental pressure profiles are displayed. Each curve shows the pressure evolution near each sensor respectively located in positions A, B and C for an electrical arc occurring in C.

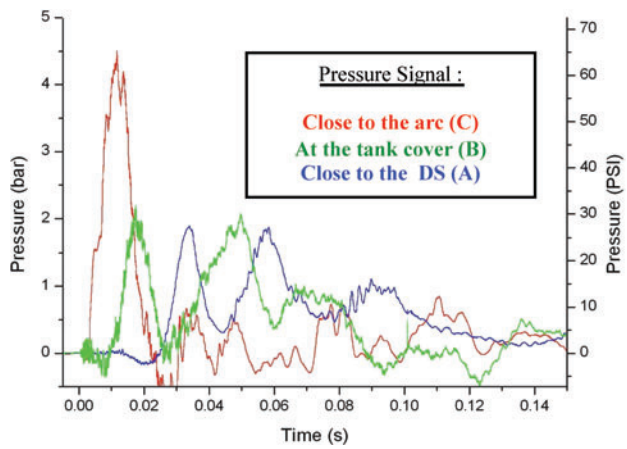

Figure 6 Pressure measurement at different locations.

The displacement of the shock wave in the tank can thus be easily followed. The arc ignition located in C causes a high-pressure peak. The pressure waves propagate leading to a second delayed lower peak in B, ending in A. For each sensor, the other pressure peaks (smaller than the main peak) are due to wave reflections off the walls. It has thus been experimentally proven that pressure is not spatially uniform in the tank, and that the pressure waves propagate at a finite speed.

3. Geometric signature

The study of the experimental pressure curves also shows that the tank structure has a local influence on the pressure behavior.

Three tests on the same transformer are compared in figure 7 and figure 8 (same arc location, but different arc energies). The time pressure behaviors during the fault are similar; a characteristic high second peak occurs.

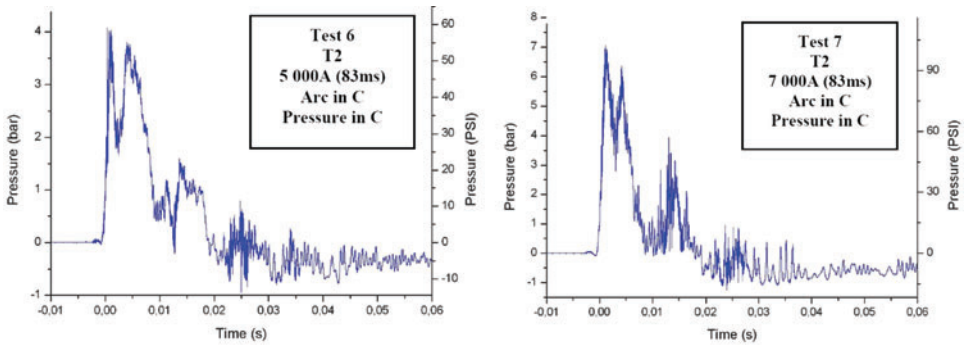

Figure 7 Pressure profiles.

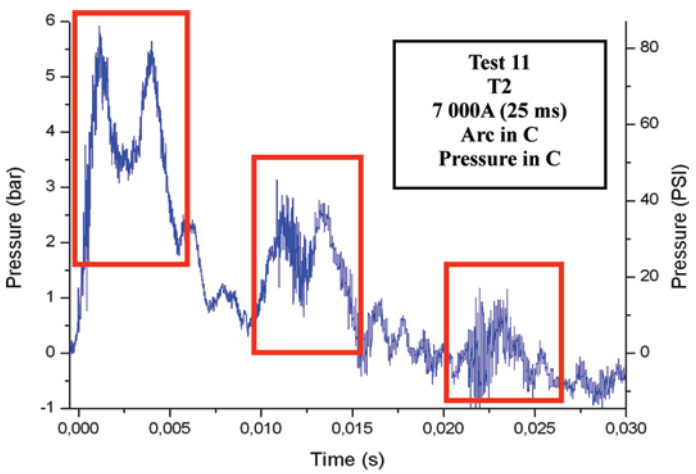

Figure 8 Pressure profiles.

As explained previously, the waves interact with the structure and reflected waves are generated. These secondary waves have the same pattern (the M-shape located with red rectangles in figure 8) meaning that the structure has a real influence on the pressure behavior. The only parameter that seems not to depend on the structure is the maximum level of pressure.

4. Pressure peaks amplitude

Only one main pressure peak has been noticed for each test. The pressure profiles show variations after that main peak but their magnitude remains low compared to the first pressure peak level.

Indeed, the initial energy transfer is almost instantaneous, and so is the phase change. The created gas has no time to expand and reach the pressure and temperature equilibrium with the surrounding oil. Because of the oil inertia that prevents the gas expansion, this gas gets very quickly under pressure, which generates the first very strong pressure waves.

As it is more difficult to vaporize a liquid than to crack oil vapor, the arc location would mainly remain in the gaseous phase after its ignition. The vaporization which happens after the gas bubble appearance is smoother and do not really generate physical conditions such as the ones in the very first arc instants. The secondary pressure variations are thus the result of the interacting waves and structure influence combined with the smooth gas generation influence on pressure.

The peaks range from *+1.5 bar* to *+13 bar* (*+21.75* to *+188.55 psi*) for arc energies from *0.01 MJ* to more than *2.4 MJ* as shown in figure 10. The maximum pressure seems to strongly increase with the arc energy while the energy remains in the low range. This dependence tends to weaken as the energy increases. The pressure rise is indeed the result of the strong oil vaporization that takes place in the arc very first moments, the energy transferred after while having less impact on the pressure build-up. As an illustration, the figure 9 shows that, when comparing tests for which pressure peaks respectively equal *+8 bar* (*+116 psi*) and *+8.8 bar* (*127 psi*), the maximum pressure only varies in *0.8 bar* (*11.6 psi*) while the corresponding arc energies vary within on order 10 of magnitude (*0.1 MJ* and *1 MJ* respectively). This is a very important statement when trying to extrapolate the pressure maximum for high energy arcs: according to the here above data, the local pressure should remain in the pressure range experienced during the CEPEL tests.

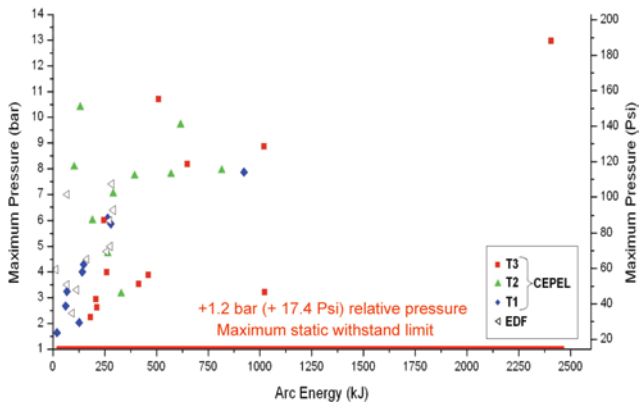

Figure 9 Maximum relative pressure close to the arc vs. arc energy (ref. pressure: atmospheric).

5. Tank withstand

To static pressure: To check the mechanical properties of the transformers, static tests were performed before applying any low impedance fault. The withstand limit was found to be *+0.7 bar* (*+10.15 psi*) for the biggest CEPEL test transformer, T3. Therefore, this limit (*+0.7 bar*, *+10.15 psi*) has been used in this analysis as a threshold for the tank depressurization during the dynamic tests. As long as the average static pressure, inside the transformer, remains under this limit, the transformer is safe.

To dynamic pressure: Even if the local pressure measured during the dynamic tests is on average 6 or 10 times higher than the static withstand limit (Figure 9), no tank damage and no tank permanent deformation occurs because the pressure peaks are of high frequency. In fact, the structure can locally withstand high dynamic pressure increases thanks to the elasticity of its walls. If the pressure had remained above the static overpressure limit, the tank would have exploded.

E. ACCELERATION

Figure 10 shows the acceleration due to the shock waves interactions with the transformer structure for an arc duration of 83 ms. The acceleration quantifies the tank movement and the fault stiffness. During these tests, for a transformer weight of *72 tons* the acceleration reached more than *400 g (g = 9.81 m/s^2 i.e. 32.2 ft/s^2)* showing that the applied faults are rather considerable.

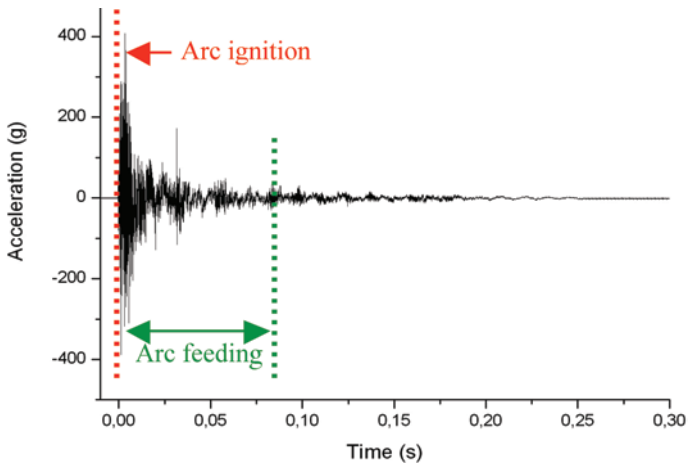

Figure 10 Tank acceleration profile—T3.

This highest acceleration is reached at the time of the creation of the electrical arc, when liquid is suddenly and intensely vaporized.

F. FAST DRAIN INFLUENCE ON THE PRESSURE EVOLUTION

1. Activation time

The "activation time" is the addition of the following times:

- The "pressure wave transit time" is the time required from the arc ignition, for the shock waves to propagate and reach the DS;
- The inertia of the DS to operate;
- And the DS burst indicator signal delay.

On average, the DS has activated after about 20 milliseconds (minimum: *4.64 ms*, maximum: *45.7 ms*) after the arc was ignited. Because the pressure wave propagation speed is finite, the maximum distance between the arc location and the DS is the parameter that matters the most for the DS to activate. In the worst situation, the arc occurs in the transformer lower part opposite the Depressurization Set (location C).

2. Depressurization time

The depressurization time is the time between the DS opening and when the pressure is definitely under the level of *+0.7 bar (+10.15 psi)*. It is reminded here that the level of *+0.7 bar* corresponds to the static pressure limit where leaks appeared on the T3 transformer during the static pressure tests. On average, the DS depressurizes the tank in *116 ms*, with a minimum value of *19.7 ms*, and a maximum of *347 ms*. This experimentally proves the DS ability to depressurize the transformer tank within tens of

milliseconds and also proves the ability of the tank to withstand dynamic pressure waves during this time.

G. CONCLUSIONS

The experiments showed that when an electrical arc occurs inside a transformer tank, it first vaporizes the surrounding oil. This gas bubble is then quickly pressurized because the liquid inertia prevents its expansion. The pressure difference between the gas bubble and the liquid oil generates dynamic pressure wave that propagates in the tank. When the pressure peak reaches the DS, it triggers the evacuation of the oil out of the transformer tank. This generates rarefaction waves that propagate through the transformer, progressively depressurizing the whole tank, thus avoiding the explosion. During the protection operation, the tanks were submitted to dynamics pressure peaks up to 14 bars abs. but did not rupture. Tanks are able to resist to very localized and dynamic pressure peaks for a very short period of time.

Besides, when subjected to static pressure (*ie* uniform pressure in the tank for a long period of time) above 2.2 bars, it ruptures.

This suggests that during a transformer explosion induced by an arcing, the rupture of the tank occurs when the dynamics pressure waves and their reflections builds up static pressure that stabilizes over the tank static withstand limit.

For safety reasons, no tests could be made without any protection and no explosion were experimented. Indeed, due to the large quantity of flammable oil contained in a transformer (up to 22 tons for the T3 transformer), a fire would be very difficult to control and extinguish. Moreover, it might last for days and even weeks.

The next step consists in presenting the development of a simulation tool that has been designed in order to:

- understand how the dynamic pressure waves generated by the arc can lead to the tank rupture,
- perform tests which could highlight the effects of a protection based on a quick oil evacuation by comparing the pressure evolution after an electrical arc inside a protected tank to the pressure evolution for the same arcing conditions inside an unprotected tank.

4. PHYSICAL MODELLING

A. BASIS

The experiments presented in the previous section showed that the key phenomena in transformers explosion and their prevention are first, the local pressure increase induced by the vaporization of the oil surrounding the arc and second, the pressure waves propagation. The core of the simulation tool then consists of a set a partial differential equations that govern the fluids dynamic while the other physical phenomena (viscosity, thermal effect, electromagnetic effects...) are modeled via the source terms added in the partial differential equations. Both phases (liquid/gas) are considered compressible. The thermodynamics of the two phases are carefully handled to prevent any theoretical or numerical problems. The modeling is dedicated to flows with interfaces so that both phases share a single pressure and velocity at a given point in the domain.

B. BIBLIOGRAPHY

Two-phase flow models used in a compressible framework can be found in the literature, largely in the detonation field where materials are subjected to extreme pressures.

Such an approach was first used by Baer & Nunziato [9] who derived the basis of a very general compressible two-phase flow model where every phase has its own pressure and velocity to depict explosions and detonations. Their work was adapted and improved to take into account the relaxation terms in order to get back to mechanical equilibrium and handle flows with interfaces [10] [11].

Based on that work, an asymptotic analysis was used to simplify the general model under the assumption that the mechanical equilibrium must be fulfilled instantaneously between phases in contact [12] [13]. This model was further improved to describe flows with gas/liquid interfaces, and proof was given for its ability to accurately describe pressure wave propagation within two-phase flows [14] [15] [16].

C. HYDRODYNAMIC GLOBAL MODEL

The following equations are used to theoretically and numerically describe the local physical phenomena:

$$\begin{cases} \dfrac{\partial \alpha_1}{\partial t} & +u.\nabla\alpha_1 & = & 0 \\ \dfrac{\partial \rho}{\partial t} & +div(\rho u) & = & 0 \\ \dfrac{\partial \alpha_1\rho_1}{\partial t} & +div(\alpha_1\rho_1 u) & = & 0 \\ \dfrac{\partial \rho u}{\partial t} & +div\left(\rho u\otimes u+P\bar{\bar{I}}\right) & = & \Phi_g^u+\Phi_\mu^u \\ \dfrac{\partial E}{\partial t} & +div((E+P)u) & = & \Phi_g^E+\Phi_\mu^E+\Phi_T^E \end{cases} \quad (1)$$

In equation (1), the terms Φ_g^u, Φ_g^E, Φ_μ^u, Φ_μ^E and Φ_T^E describe the effects of gravity (g), viscosity (μ), and thermal effects (T) on the phase velocity and energies. These terms are defined in section E of this chapter.

D. THERMODYNAMICS CLOSURE

Each fluid has its own thermodynamic behavior as it is described by its own Equation of State (EOS). Thus, for completeness and consistency an added thermodynamic closure links the mixture pressure to the total mixture energy. Therefore an EOS exists for the whole mixture to deal with smeared interfaces between oil and gas due to diffusion from the numerical method.

The EOS for the entire mixture is both simple and robust. It only relies on two state parameters: the polytrophic coefficient γ and the stiffness parameter π. Thus, the behaviors of gasses, liquids and solids are accurately described. Also, these parameters facilitate simple calculations to determine the speed of sound in the media. Fluid Pressure and internal energy are linked by the EOS given in equation (2).

$$P=(\gamma-1)\rho\varepsilon-\gamma\pi \quad (2)$$

E. GRAVITY, VISCOUS AND THERMAL EFFECTS

In the equation (1) the various terms Φ_g^u, Φ_g^E, Φ_μ^u, Φ_μ^E and Φ_T^E are defined by equation (3).

$$\begin{cases} \Phi_g^u = \rho u \\ \Phi_g^E = \rho\, u.g \\ \Phi_\mu^u = div\left(\mu \overline{\overline{\tau}}\right) \\ \Phi_\mu^E = div\left(\mu \overline{\overline{\tau}}.u\right) \\ \Phi_T^E = \sum_k \alpha_k div\left(K_k \nabla T_k\right) \end{cases} \tag{3}$$

Finally, the viscous mixture stress tensor, $\overline{\overline{\tau}}$, and the deformation rate tensor, $\overline{\overline{D}}$, are defined by equation (4).

$$\begin{cases} \overline{\overline{\tau}} = -\dfrac{2}{3} div(u)\,\overline{\overline{I}} + 2\overline{\overline{D}} \\ \overline{\overline{D}} = \dfrac{1}{2}\left(\overline{\overline{grad}}\ u + \overline{\overline{grad}}^{t}\ u\right) \end{cases} \tag{4}$$

5. NUMERICAL METHOD

A 3D finite element method enables numerical solutions for the PDEs described by the physical model. The third dimension can be omitted, with derivatives in the third dimension set to zero, if a 2D model is desired.

A. MESH DESCRIPTION

In order to perform numerical simulations, the physical geometry is split into small calculation cells wherein physical values are assumed to be constant throughout the cell volume. The transformer is discretized into finite volumes via an unstructured mesh. The walls, windings and transformer core are all modeled as rigid obstacles which interact with the pressure waves.

B. PDE ANALYSIS

Based on the hydrodynamic equations (1), the physical model can be written in the following compact form.

$$\frac{\partial W}{\partial t} + \frac{\partial F(W)}{\partial x} + \frac{\partial G(W)}{\partial y} + \frac{\partial H(W)}{\partial z} + M_x(W) + M_y(W) + M_z(W) = 0$$

Where :

$$W^t = \left[\ \alpha_1, \rho, \alpha_1\rho_1, \rho u, \rho v, \rho w, E\right]$$

$$F^t(W) = [0,\ \rho u,\ \alpha_1\rho_1 u,\ \rho u^2 + \boldsymbol{P},\ \rho uv,\ \rho uw,\ (E+P)u]$$

$$G^t(W) = [0,\ \rho v,\ \alpha_1\rho_1 v,\ \rho uv,\ \rho v^2 + P,\ \rho vw,\ (E+P)v]$$

$$H^t(W) = [0,\ \rho w,\ \alpha_1\rho_1 w,\ \rho uw,\ \rho vw,\ \rho w^2 + P,\ (E+P)w]$$

$$\begin{aligned} M_x^t(W) &= [u\frac{\partial \alpha_1}{\partial x},\ 0,\ 0,\ 0,\ 0,\ 0,\ 0] \\ M_y^t(W) &= [v\frac{\partial \alpha_1}{\partial y},\ 0,\ 0,\ 0,\ 0,\ 0,\ 0] \\ M_z^t(W) &= [w\frac{\partial \alpha_1}{\partial z},\ 0,\ 0,\ 0,\ 0,\ 0,\ 0] \end{aligned} \tag{5}$$

As with every PDE system, we can associate a Jacobian matrix to the set of equations, and the matrix of our PDE system once projected on the local coordinate system is thus:

$$A_n(Y) = \begin{pmatrix} u_n & 0 & 0 & 0 & 0 & 0 & 0 \\ 0 & u_n & 0 & \rho n_x & \rho n_y & \rho n_z & 0 \\ 0 & 0 & u_n & \alpha_1\rho_1 n_x & \alpha_1\rho_1 n_y & \alpha_1\rho_1 n_z & 0 \\ 0 & 0 & 0 & u_n & 0 & 0 & \frac{n_x}{\rho} \\ 0 & 0 & 0 & 0 & u_n & 0 & \frac{n_y}{\rho} \\ 0 & 0 & 0 & 0 & 0 & u_n & \frac{n_z}{\rho} \\ 0 & 0 & 0 & \rho c^2 n_x & \rho c^2 n_y & \rho c^2 n_z & u_n \end{pmatrix} \tag{6}$$

The PDE system analysis can then be performed on this matrix to find the mathematical properties of the physical model. The eigenvalues are of utmost importance in problems of this kind. Here, we have three eigenvalues:

$$\begin{cases} \lambda_1 = u_n - c \\ \lambda_2 = u_n \\ \lambda_3 = u_n + c \end{cases} \tag{7}$$

The orders of multiplicity are, respectively, 1, 5, and 1. It can be shown that λ_1 and λ_3 are acoustic waves (typically rarefaction waves and shocks), whereas λ_2 is a contact discontinuity. The associated Riemann problem is thus very similar to the one associated with Euler equations [17] [18] [19]. The corresponding right eigenvectors can be calculated:

$$\begin{cases} R_1^t = \left[0, \rho, \alpha_1\rho_1, -cn_x, -cn_y, -cn_z, \rho c^2\right] \\ R_{21}^t = \left[1,0,0,0,0,0,0\right] \\ R_{22}^t = \left[0,1,0,0,0,0,0\right] \\ R_{23}^t = \left[0,0,1,0,0,0,0\right] \\ R_{24}^t = \left[0,0,0,-n_y, n_x, 0, 0\right] \\ R_{24}^t = \left[0,0,0,-n_z, 0, n_x, 0\right] \\ R_3^t = \left[0, \rho, \alpha_1\rho_1, cn_x, cn_y, cn_z, \rho c^2\right] \end{cases} \tag{8}$$

A more detailed analysis shows that the dimensions of the eigenspace associated with every eigenvalue is equal to the eigenvalue's multiplicity, which means that the PDE system is hyperbolic and can be numerically solved using the usual dedicated numerical methods.

C. FINITE VOLUME SCHEME FOR CONSERVATIVE ASPECTS

We then apply a Finite Volume Method onto the system over a cell Ω with a time step to Δt derive:

$$\iint_{\Omega_i \Delta t} \frac{\partial W}{\partial t} d\Omega\, dt + \iint_{\Omega_i \Delta t} \left(\frac{\partial F(W)}{\partial x} + \frac{\partial G(W)}{\partial y} + \frac{\partial H(W)}{\partial z} \right) d\Omega\, dt = 0 \tag{9}$$

The numerical scheme for the conservative part of the hydrodynamic model finally reads

$$\Omega_i \left(W_i^{n+1} - W_i^n \right) + \Delta t \sum_{j \in V(i)} \Psi\left(W_{ij}^n \right).n_{ij} S_{ij} = 0$$

Where:

$$\Psi(W_{ij}).n_{ij} = F\left(W_{ij}\right) n_{x_{ij}} + G\left(W_{ij}\right) n_{y_{ij}} + H\left(W_{ij}\right) n_{z_{ij}} \tag{10}$$

The quantity $\Psi(W_{ij}).n_{ij}$ describes the numerical flux at the cell boundary between cells i and j. It must be evaluated at each cell-boundary.

D. FINITE VOLUME SCHEME FOR NON CONSERVATIVE ASPECTS

The gas volume fraction behaves according to an advection equation. Several ways to handle such terms are noted in the literature, but the Godunov numerical scheme [18] for an advection equation has been chosen to solve our problem:

$$\alpha_i^{n+1} = \alpha_i^n - \frac{\Delta t}{\Omega_i} \sum_{\mathrm{j} \in V(i)} \left(\alpha_{ij}^n - \alpha_i^n \right) u_{ij}^n .n_{ij}\, S_{ij} \tag{11}$$

This discretization scheme is numerically robust and very stable.

E. GRAVITY, VISCOUS AND THERMAL EFFECTS

Where φ is any physical variable, $\varphi*$ represents any intermediate temporal state between the two instants n and $n + 1$.

1. Gravity

The gravity source terms are taken into account by a time splitting scheme. The resulting numerical scheme, based on a first order Runge-Kutta time scheme is thus:

$$\begin{cases} \alpha_i^* = \alpha_i^n \\ \rho_i^* = \rho_i^n \\ \left(\alpha_1\rho_1\right)_i^* = \left(\alpha_1\rho_1\right)_i^n \\ u_i^* = u_i^n + \Delta t.g_x \\ v_i^* = v_i^n + \Delta t.g_y \\ w_i^* = w_i^n + \Delta t.g_z \\ E_i^* = E_i^n + \rho_i^n \Delta t\left(g_x.u_i^n + g_y.v_i^n + g_z.w_i^n\right) \end{cases} \quad (12)$$

2. Viscous and thermal effects

The contributions from the viscous and the thermal effects are obtained in a similar fashion as the hydrodynamic part. The associated numerical scheme is thus:

$$\begin{cases} \alpha_i^* = \alpha_i^n \\ \rho_i^* = \rho_i^n \\ \left(\alpha_1\rho_1\right)_i^* = \left(\alpha_1\rho_1\right)_i^n \\ \rho u_i^* = \rho u_i^n + \dfrac{\Delta t}{\Omega_i}\displaystyle\sum_{j\in V(i)} \mu_{ij}^n \bar{\bar{\tau}}_{ij}^n.\vec{n}_{ij}S_{ij} \\ E_i^* = E_i^n + \dfrac{\Delta t}{\Omega_i}\left(\displaystyle\sum_{j\in V(i)} \mu_{ij}^n\left(\bar{\bar{\tau}}_{ij}^n.u_{ij}^n\right).\vec{n}_{ij}S_{ij} + \sum_k \alpha_{ki}^n \sum_{j\in V(i)}\left(K_k\nabla T_k^n\right)_{ij}.\vec{n}_{ij}S_{ij}\right) \end{cases} \quad (13)$$

The velocity gradients $\left(\overline{\overline{grad}\,u}\right)_{ij}$ and consequently the viscous stress tensor $\bar{\bar{\tau}}_{ij}$ as well as the dynamic viscosity μ_{ij} are evaluated at each cell boundary. The evaluation method is the one used in [20]. The temperature gradients $\left(\nabla T_k\right)_{ij}$ are evaluated the same way as the velocity gradients are. Note that here we do not work with the mixture temperature to compute thermal contributions due to heat conduction.

F. RIEMANN PROBLEMS AND SOLVERS

A Riemann problem consists of a Partial Differential Equation (PDE) set with initial conditions that are uniform on both sides of an initial single discontinuity. Time evolution of such problems can be described when introducing wave concepts. Details about Riemann problems, their adaptation and their solving can be found in [17] [18] [19].

1. Riemann solvers

At every time step in a Finite Volume Method, there exists a variable discontinuity at cell boundaries as a natural consequence of discretization. In order to find the appropriate values of the variables at a given cell boundary, a Riemann problem must be solved using dedicated Riemann solvers. The flux of the variables W_{ij}, denoted $\Psi\left(W_{ij}\right).\vec{n}_{ij}$, is given as a solution from the Riemann problem between cells Ω_i and Ω_j.

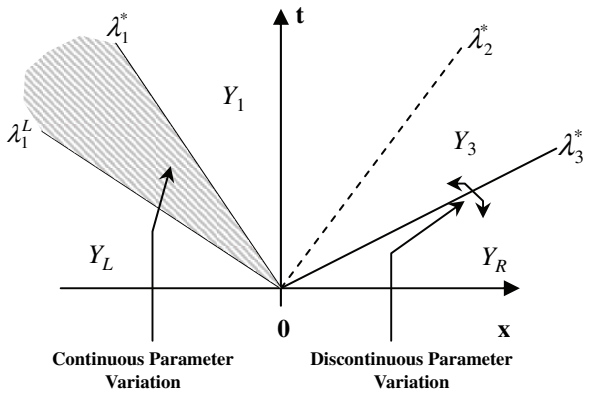

Figure 11 Riemann problem illustration.

Dedicated Riemann solvers are divided into three main categories: Some exactly solve an exact Riemann problem (Godunov Solver [18] [19]), others exactly solve an approximate Riemann problem (VFRoe [17], acoustic solvers [19]), while the last category provides approximate solutions for approximate Riemann problems.

An exact solver for exact Riemann problems has been built for the working model. Following the rules detailed in [19], when presenting the Godunov solver for Euler equations we can also build an exact solver for our model. The various state expressions can be deduced from those of [19] and are not recalled in the present document.

2. Boundary treatment

Boundary conditions accurately model the physical interaction between fluids and structures. Virtual cells are created just past the limit of the physical geometry, and boundary conditions are satisfied by carefully setting the values within the virtual cells.

Once the virtual cells are updated with new variables, a Riemann problem is solved at the interface between the real and the virtual cell, and the results are processed no differently than those obtained between two real cells [22].

Several types of boundary conditions are considered in the present work:

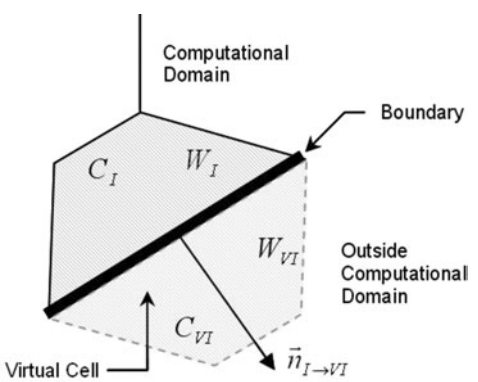

Figure 12 Boundary treatment in a 2D framework.

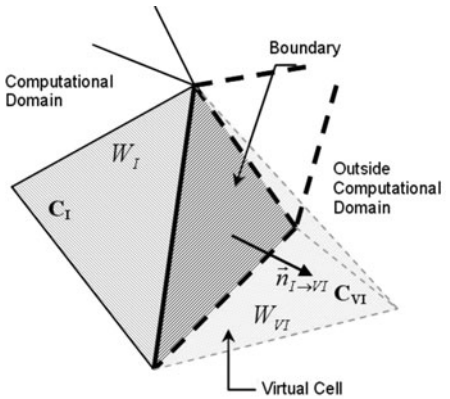

Figure 13 Boundary treatment in a 3D framework.

3. Imposed boundaries

For imposed boundary conditions, the virtual cell is set with a reference state, which remains constant from time step to another.

4. Absorption boundaries

Absorption boundary conditions are created by having the virtual cell copied from the current state of the neighbouring cell inside the physical domain.

5. Slipping and non-slipping walls

Slipping and no-slipping wall boundary conditions are the most commonly used boundary conditions. In the following, U_n is the normal velocity to the wall evaluated at the wall and U_{t1} and U_{t2} are the two tangential velocities to the wall evaluated at the wall. The virtual state is set such that the fluid cannot go through the boundary by ensuring that $U_n = 0$. To achieve such a goal, and knowing the inner domain state $W_I = (\alpha_I, \rho_I, \alpha_{1I}\rho_{1I}, U_{nI}, U_{t1I}, U_{t2I}, P_I)^t$, the virtual state is defined as:

$$W_{VI} = (\alpha_I, \rho_I, \alpha_{1I}\rho_{1I}, -U_{nI}, U_{t1I}, U_{t2I}, P_I)^t.$$

If viscosity effects are taken into account, the velocity at the wall must be zero, therefore:

$$W_{VI} = (\alpha_I, \rho_I, \alpha_{1I}\rho_{1I}, -U_{nI}, -U_{t1I}, -U_{t2I}, P_I)^t.$$

6. Subsonic inlets and outlets

Automatic subsonic inlet/outlet boundary conditions are a little more complicated. We recall that the normal vector to the boundary always heads outward the physical domain. However, we can see in figure 3 below that two out of three waves are located on the same side of the boundary, making it difficult to determine the virtual state.

In order to get analytical expressions easily handled in a calculation or by CFD codes, it is assumed that shocks can be described by an isentropic compression.

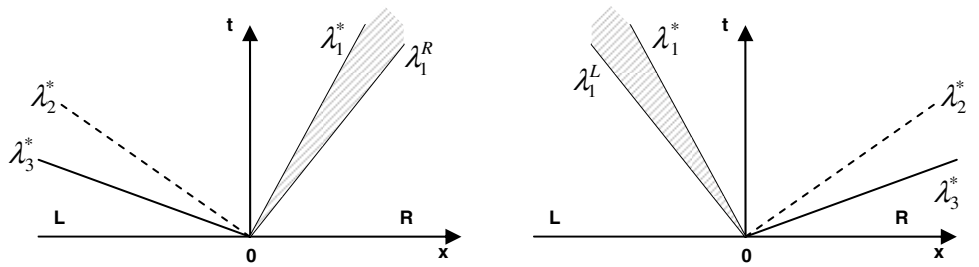

Figure 14 Subsonic inlet (left) and outlet (right).

The sought state is noted $\varphi*$. Then, one of the boundary cell edge variables is set arbitrarily—most of the time the pressure p*—and the Riemann invariants across the different waves are combined to get the sought parameters. For the present model, the Riemann invariants are defined by equations (14) and (15) (subscript φ_I stands for the inner computational domain variables, and the subscript φ_0 for the state reference).

Subsonic outlet:

$$\begin{cases} p^* = p_{imposed} \\ \alpha^* = \alpha_I \\ \rho^* = \rho_I \left(\dfrac{p^* + \pi(\alpha^*)}{p_I + \pi_I} \right)^{\frac{1}{\gamma(\alpha^*)}} \\ \rho_g{}^* = \rho_{gI} \left(\dfrac{p^* + \pi(\alpha^*)}{p_I + \pi_I} \right)^{\frac{1}{\gamma(\alpha^*)}} \\ U_n{}^* = U_{nI} + 2\dfrac{c_I - c^*}{\gamma_I - 1} \\ U_{t1}{}^* = U_{t1I} \\ U_{t2}{}^* = U_{t2I} \end{cases} \quad (14)$$

Subsonic inlet:

$$\begin{cases} p^* = p_{imposed} \neq p_0 \\ \alpha^* = \alpha_0 \\ \rho^* = \rho_0 \left(\dfrac{p^* + \pi(\alpha^*)}{p_0 + \pi_0} \right)^{\frac{1}{\gamma(\alpha^*)}} \\ \rho_g{}^* = \rho_{g0} \left(\dfrac{p^* + \pi(\alpha^*)}{p_0 + \pi_0} \right)^{\frac{1}{\gamma(\alpha^*)}} \\ U_n{}^* = U_{n0} - 2\dfrac{c_0 - c^*}{\gamma_0 - 1} \\ U_{t1}{}^* = U_{t10} \\ U_{t2}{}^* = U_{t20} \end{cases} \quad (15)$$

The inner pressure and an imposed external state is used to calculate respectively the outlet and inlet virtual states.

6. COMPARISONS SIMULATIONS/EXPERIMENTS

This section compares the results from the simulations with the experimental data for the same transformer geometry and arcing conditions in order to check the ability of the tool to describe transformer explosion and their prevention. Once validated, the computational tool is then used to analyze the effects on an unprotected transformer of the arcing conditions used during the experimental campaign.

A. EXPERIMENTS / SIMULATIONS: QUALITATIVE RESULT COMPARISON

Simulation results and experimental data have been compared. In this section, comparisons for tests 31 and 33 which conditions are detailed in Table 1 are displayed in Figure 15 and Figure 16. The transformer geometry used for this study is the T3 transformer (*5.3 m × 3.8 m × 2.6 m ie 17.4 ft × 12.5 ft × 8.6 ft*).

Table 1 Tests retained for comparisons between experiments and simulations

Test Number	**31**	**33**	**23**	**24**
Arc Position	B	B	B	C
Arc Duration (*ms*)	83	83	83	83
Maximal Current (*A*)	34 476	14 476	13 121	31 783
Maximal Voltage (*V*)	1034	979	860	923
Arc Energy (*kJ*)	460	212	208	414

Experimental and numerical results regarding the pressure time evolution are similar. In both cases, the three same phases can be observed: (phase 1), a very sharp pressure rise following the arc ignition, (phase 2) a pressure drop because of the protection activation, and (phase 3) the pressure alternatively rises and decreases because of the complex wave dynamics due to the wave reflections off the transformer walls (cf. figure 15 and figure 16). It can be checked that in both cases the pressure gets back to the initial reference pressure.

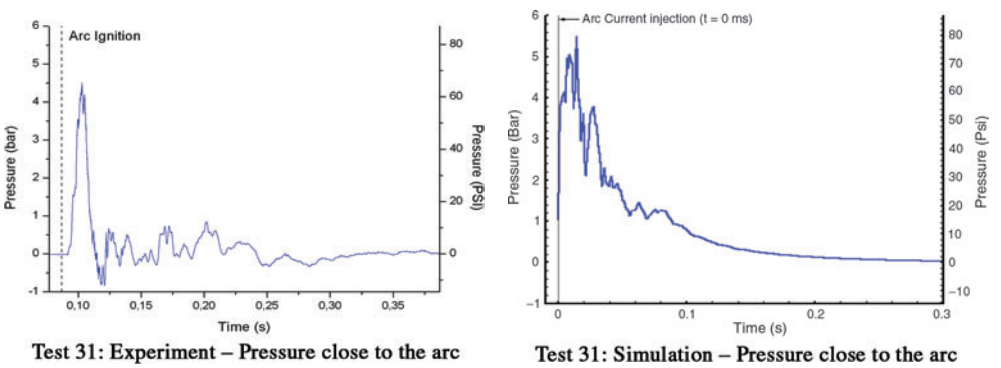

Figure 15 Experiments / Simulation pressure profiles comparison.

In figure 15 and figure 16 where numerical as well as experimental results are displayed, the experimental results are in accordance with the tendency exhibited in the previous sections. The computer simulated pressure profiles are very similar as well: even if the pressure maxima are not exactly the same, the chronology of the phenomena and the profile shapes are similar.

These similarities between experiments and theory confirm the geometry influence on local pressure profiles. On each profile, we can also notice that the fast drain influence causes an inner tank average pressure decrease. The pressure oscillations are due to the pressure waves (rarefaction and compression waves) which propagate back and forth in the tank interacting with the tank structure.

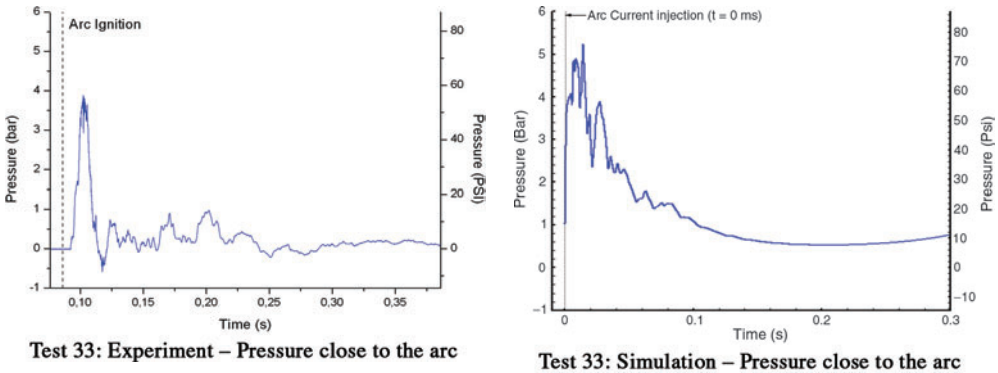

Figure 16 Experiments/simulation pressure profiles comparison.

B. EXPERIMENTS / SIMULATION: QUANTITATIVE RESULT COMPARISON

Experimental as well as simulated pressure peaks have been quantitatively compared. In Table 2 we display this comparison for 4 tests (numbered 23, 24, 31 and 33, see conditions in Table 1). The relative error shows that the simulations and the experiments are in very good agreement.

Table 2 Pressure peaks comparison

Tests	**Relative error**	**Absolute pressure peak close to the arc (simulation)**		**Absolute pressure peak close to the arc (experiment)**	
		bar	*psi*	*bar*	*psi*
23	**6 %**	5.03	73	5.31	77
24	**15 %**	3.45	50	3	43.5
31	**1.2 %**	5.5	80	5.45	79
33	**7.4 %**	5.24	76	4.88	70.76

Regarding the comparisons between the simulation results and the experimental data, the numerical environment is thus a reliable tool to predict the consequences of a low impedance fault occurring in a transformer.

Experimental testing would be dangerous if the transformer is not protected by any protection so numerical simulations were performed instead of live tests. Figure 13 shows pressure evolutions computed for a geometry and for arcing conditions similar to those of the CEPEL test 31 (Figure 15). It shows that, after the arc feeding, the average pressure remains close to an equilibrium state equal to *7 bar (100 psi)*, much higher than the static withstand limit pressure.

Thus, during test 31, if the transformer had not been equipped with the TP, the inner average pressure would have risen up to the static overpressure withstand limit (*2.2 bars, 31.9 bars*). The transformer would have exploded as soon as the tank wall elasticity limits were over, i.e. as soon as the tank walls could not store any more mechanical energy due to the pressure increase.

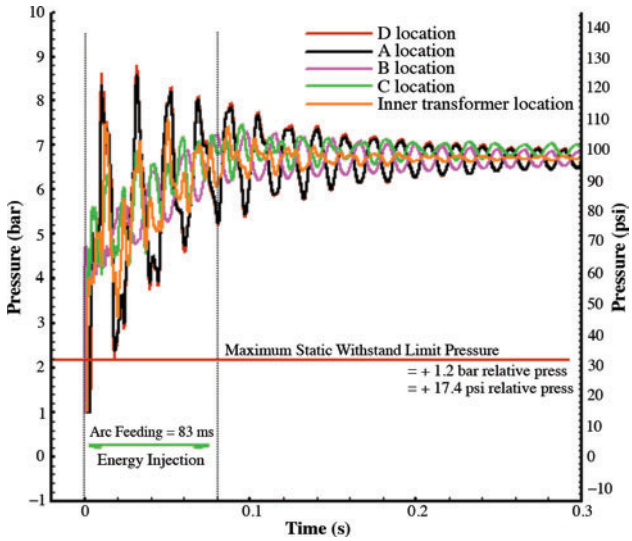

Figure 17 Pressure evolution when the tank is not protected.

7. APPLICATION TO THE PROTECTION OF A 200 MVA TRANSFORMER

A. AIM OF THE STUDY

The present section thus uses the simulation tool in order to study in details the effects of a pressurised gas bubble generated by an electrical arc occurring in a usual 200 MVA transformer. Moreover, it analyses the consequences of using the strategy presented in the first section to prevent transformer tank explosion.

B. CONFIGURATIONS

The 200 MVA transformer is *5.75 m* long, *3.25 m* high and *2.5 m* large and all the equipments of the transformers, such as bushing turrets or windings are taken into account. An electrical arc (*11.5 MJ*-arc generating about *3.4 m*^{3} of gas) ignites near a winding, generating an *11 bar abs* gas bubble.

C. RESULTS OF THE SIMULATIONS

Figure 2 shows the simulated evolution of the pressure inside the tank after the occurrence of the gas bubble generated by the arc. On the left side (fig. 18a), the transformer is equipped with the protection presented in the previous paragraph, while on the right side (fig. 18b), the transformer is not protected against overpressure.

When the transformer is equipped with the protection, the pressurized gas bubble creates pressure waves which propagate throughout the transformer, reflecting and otherwise interacting with the tank structure (fig. 18b). Within *3 ms*, a large pressure peak has reached the entry of the first bushing, as shown in fig. 18b. Then the pressure wave triggers the Depressurization Set activation within about *10 ms* after the gas bubble creation. This induces the rapid evacuation of fluid from the transformer tank, which thus generates rarefaction waves spreading throughout the transformer. After only *60 ms*, the pressures throughout the transformer stabilize well below dangerous levels, as shown in fig. 18b.

Otherwise, when the tank is not equipped with any protection system, and if it is subjected to a similar low impedance fault, the tank is exposed to very dangerous pressure levels. For instance, *30 ms* after the arc occurrence, the pressure in a bushing reaches more than *10 bars* abs as shown in figure 18a. Moreover, without the tank protection, the static pressure stabilizes around *6 bars abs* and the transformer would violently explode (as transformer tanks are designed to withstand static pressure up to about *2.2 bars abs*).

8. CONCLUSIONS

An experimental tests campaign was dedicated to the understanding of transformers explosion induced by electrical arcing.

Because transformer explosions are uncontrollable and lead to huge damages, the tests were performed with transformers equipped with an explosion prevention technology that reacts to dynamic pressure peaks.

The tests showed that when an electrical arc occurs in the tank, the oil surrounding the arc is quickly vaporized and the generated gas is pressurized because the liquid inertia prevents its expansion. The pressure difference between the gas bubbles and the surrounding liquid oil generates pressure waves that propagate through the oil. When the first dynamic pressure peak reached the protection, it triggered an oil evacuation that quickly depressurized the tank so that no tank rupture occurred.

During the tests, transformer tanks could withstand such high pressure peaks (up to 14 bars abs.) during several tens of milliseconds even if the static withstand limit of transformer tanks is around 2.2 bars abs.

Complementarily, the consequences of arcing inside unprotected transformers can be studied safely using computational simulations. A numerical simulation tool was developed for that purpose. In order to be efficient, it has to deal with liquid and gas and to be able to compute pressure wave propagations.

Therefore, a complete modeling for unsteady compressible two phase flows has been adapted and a finite volume method was set to solve the equations on 3D unstructured meshes. The experimental tests' results were used to validate the computer simulation tool by comparison with experiments.

Simulations were then run on a 200 MVA transformer; they highlighted the advantages of using advanced simulation tools:

- First, it gives a deep understanding of what happens during a transformer explosion. The simulation tool confirmed that when an electrical arc occurs insides a transformer tank that is not protected, the dynamic pressure waves generated by the arc propagate through the tank, reflects on the wall and progressively increases the static pressure inside the tank resulting in its rupture.
- Second, the computational tool is efficient to study the operation of explosion prevention strategies such as the ones based on a fast depressurization induced by oil evacuation. Indeed, the results showed that this fast fluid evacuation generates large rarefaction waves that propagate and depressurize the whole tank within milliseconds thus avoiding the static pressure build up that can not be withstood by the tank.

Such strategies can thus be considered an efficient first step in a global chain of protections against transformer explosion.

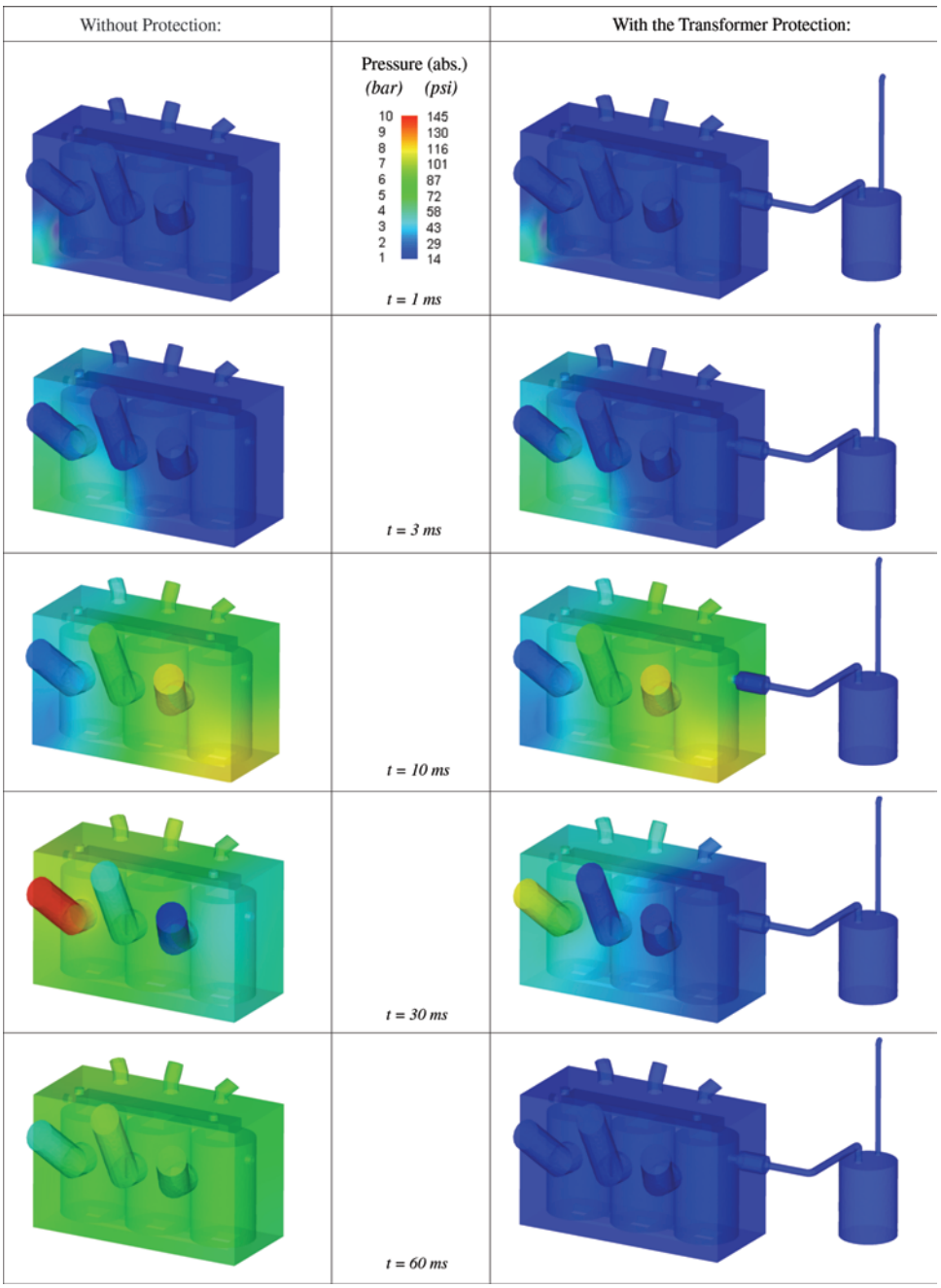

Figure 18a Pressure evolution in an unprotected tank.

Figure 18b Pressure evolution in a transformer tank equipped with a DS.

REFERENCES

[1] O.R. HANSEN, "SEBK Project: Results from Phase 2 Laboratory Scale Experiments", Gexcon, May 2001.

[2] O.R. HANSEN, A. WIIK, B. WILKINS, "SEBK project phase 4 & 5, Transformer explosion and suppression: Large scale hybrid hydrogen and transformer oil explosions with & without suppression", 2001.

[3] S. MULLER, R. BRADY, G. de BRESSY, P. MAGNIER, G. PERIGAUD, "Prevention of transformer tank explosion, Part 1: Experimental Tests on Large Transformers", ASME PVP08 Conference, 2008.

[4] W.R. MAHIEU, "Prevention of High Fault Ruptures of Pole-Type Distribution Transformers", IEEE Transactions on Power Apparatus Systems, Vol Pas-94, 1975.

[5] T. KAWAMURA, M. UEDA, K. ANDO, T. MAEDA, Y. ABIRU, M. WATANABE, K. MORITSU, "Prevention of Tank Rupture Due to Internal Fault of Oil Filled Transformers", CIGRE, 12-02, 1988.

[6] M. FOATA, M. IORDANESCU, C. HARDY, "Computational Methods for the Analysis of Explosions in Oil-Insulated Electrical Equipments", IEEE Transactions on Power Systems, Vol. 3, No. 1, 1988.

[7] J.-B. DASTOUS, M. FOATA, A. HAMEL, "Estimating Overpressures in Pole-Type Distribution Transformers Part II: Prediction Tools", IEEE Transactions on Power Delivery, Vol. 18, No. 1, 2003.

[8] G. PERIGAUD, G. BRESSY, S. MULLER, R. BRADY, P. MAGNIER, "Numerical Investigations to Prevent Transformer Tank Explosion", Australia, TechCon Asia Pacific 2008.

[9] M.R. BAER & J.W. NUNZIATO, "A Two-phase Mixture Theory for the Deflagration to Detonation Transition in Reactive Granular Materials", Intern. J. of Multiphase Flow, vol. 12, 6, pp. 861–889, 1986.

[10] R. SAUREL, R. ABGRALL, "A multi-phase Godunov Method for Compressible Multi-fluid and Multi-phase flows", Journal of Computational Physics, vol. 150, pp. 425–467, 1999.

[11] R. SAUREL & O. LEMETAYER, "A Multi-phase Model for Compressible Flows with Interfaces, shocks, detonation waves and cavitation", Journal Of Fluid Mechanics, vol. 431, pp. 239–271, 2000

[12] A.K. KAPILA, R. MENIKOFF & D.S. STEWART, "Two-phase Modelling of Deflagration to Detonation Transition in Granular Materials: Reduced Equations", Physics of Fluids, vol. 113, 10, pp. 3002–3024, 2001.

[13] A. MURRONE & H. GUILLARD, "A Five Equation Reduced Model for Compressible Two-phase Flow Problems", Journal of Computational Physics, vol. 202, Issue 2, 2005.

[14] G. ALLAIRE, S. CLERC & S. KOKH, "A Five Equation Model for the Simulation of Interfaces between Compressible Fluids, Journal of Computational Physics, vol. 181, 2, pp. 577–616, 2002.

[15] J. MASSONI, R. SAUREL, B. NKONGA & R. ABGRALL, "Eulerian model and method proposal for flows with interfaces in presence of heat transfers", International Journal Of Heat and Mass Transfers, vol. 45, 6, pp. 1287–1302, 2002.

[16] R. SAUREL, R. ABGRALL, "A Simple Method for Compressible Multi-fluid Flows", SIAM J. of Scien. Comput., vol. 21, 3, pp. 1115–1145, 1999.

[17] G. BRUN, J.M. HERARD, D. JEANDEL & M. UHLMANN, "An Approximate Roe-type Riemann Solver for a Class of Realizable Second Order Closures", International Journal of Fluid Dynamics, vol. 13, 3, pp. 223–249, 2000.

[18] S.K. GODUNOV, “A Finite Difference Method for Numerical Computation of Discontinuous Solutions of the Equations of Fluid Dynamics”, Math Sb., vol. 47, pp. 357–393, 1959.

[19] E. TORO, “Riemann Solvers and Numerical Methods for Fluid Dynamics”, Press, ed. Springer Verlag, Berlin, 1997.

[20] N. THEVAND, “Contribution à l’Etude Numérique des Ecoulements Instationnaires et Visqueux de Mélanges Gaz-Particules Dilués”, Ph. D. Thesis, Université de Provence, Méchanics & Energy, Marseille, France, 1999.